ADVANCED MATERIALS
www.advmat.de

High-Detectivity Multilayer MoS_2 Phototransistors with Spectral Response from Ultraviolet to Infrared

Woong Choi, Mi Yeon Cho, Aniruddha Konar, Jong Hak Lee, Gi-Beom Cha, Soon Cheol Hong, Sangsig Kim, Jeongyong Kim, Debdeep Jena, Jinsoo Joo, and Sunkook Kim**

Recently, one of the transition metal dichalcogenides MoS_2 has generated substantial interest as a promising channel material for field-effect transistors (FETs), because of its intriguing electrical[1,2] and optical properties.[3] For example, FETs using single layer MoS_2 exhibited a high current ON/OFF ratio (~10^8) and a low subthreshold swing (SS, ~70 mV $decade^{-1}$) with an electron mobility of ~200 $cm^2V^{-1}s^{-1}$ in an $HfO_2/MoS_2/SiO_2$ dielectric environment.[1] In addition, single layer MoS_2 transistors exhibited a higher photoresponsivity (7.5 mAW^{-1}) than graphene FETs, presenting a potential application as a photo transistor.[3] Yet, the fabrication demands and the physics of MoS_2, among other reasons, suggest that multilayer MoS_2 may be more attractive than single layer MoS_2 for FET applications in a thin-film transistor (TFT) configuration.[4] For example, the synthesis of single layer MoS_2 followed by the deposition of an additional high-*k* dielectric layer may not be well-suited for commercial fabrication processes. In addition, the density of states in multilayer MoS_2 is three times higher than in single layer MoS_2, which can produce considerably high drive currents in the ballistic limit.[5] In long-channel TFTs, multiple conducting channels can be created by field-effects in multilayer MoS_2, which can boost the current drive of TFTs, similar to silicon-on-insulator MOSFETs. Moreover, multilayer MoS_2 offers a wider spectral response than single layer MoS_2 – from ultraviolet (UV) to near infrared (NIR) wavelengths – due to its narrower bandgap, which can be advantageous in a variety of photodetector applications.[6] However, multilayer MoS_2 and the corresponding dichalcogenide semiconductors have not been extensively studied for use in electronics or optoelectronics.[7,8] The characteristics in the few early reports[9,10] are not particularly competitive with current TFT technologies.

Therefore, in this work, we further explore the optoelectronic properties of multilayer MoS_2 TFTs and show a compelling case of multilayer MoS_2 phototransistors for applications in photodetectors. In particular, the interesting optoelectronic properties of our multilayer MoS_2 phototransistors could potentially lead to their integration into touch screen panels for flat panel or flexible display devices. Since the presence of external millimeter-scale touch-detecting devices (e.g., using capacitive or resistive touch sensors) in touch screen panels significantly degrades the image quality and brightness of these display devices, integration of sub-micrometer phototransistors into touch screen panels has been suggested as a way of minimizing the degradation.[11] While several semiconductors, including amorphous InGaZnO, have been reported for uses as phototransistors in touch screen panels,[12] problems, such as high power consumption and reliability, remain due to their high gate bias (>10 V), high SS (>100 mV $decade^{-1}$) and notable shift (a few V) in the threshold voltage during illumination. In contrast, our multilayer MoS_2 phototransistors with an atomic-layer-deposited (ALD) Al_2O_3 gate dielectric layer in a bottom gate TFT configuration achieve high room temperature mobilities (>70 $cm^2V^{-1}s^{-1}$), a low operating gate bias (<5 V), and a negligible shift in the threshold voltages during illumination. Furthermore, our multilayer MoS_2 phototransistors exhibit better optoelectronic properties than single layer MoS_2 phototransistors, including a wider spectral response (<~900 nm) and higher photoresponsivity (>100 mAW^{-1}).

Before fabricating the MoS_2 phototransistors, we first measured the optical absorption in multilayer MoS_2 flakes with different thicknesses across the visible and near-infrared (NIR) spectral ranges (**Figure 1**(a)). The thicknesses of MoS_2 flakes measured by a tapping mode atomic force microscopy (AFM) are ~40 nm, ~4 nm, and ~1 nm, in sequence. Regardless of their thicknesses, all of the MoS_2 flakes show two excitonic

Dr. J. H. Lee, Prof. S. Kim
Department of Electronics and Radio Engineering
Institute for Laser Engineering
Kyung Hee University
Gyeonggi, 446-701, South Korea
E-mail: intel0616@gmail.com
Prof. W. Choi
School of Advanced Materials Engineering
Kookmin University
Seoul 136-702, South Korea
Dr. M. Y. Cho, Prof. J. Joo
Department of Physics
Korea University
Seoul 136-713, South Korea
E-mail: jjoo@korea.ac.kr
Dr. A. Konar, Prof. D. Jena
Department of Electrical Engineering
University of Notre Dame
Notre Dame, Indiana 46556, USA
Dr. G.-B. Cha, Prof. S. C. Hong
Department of Physics and Energy Harvest-Storage Research Center
University of Ulsan
Ulsan 680-749, South Korea
Prof. J. Kim
Department of Physics
University of Incheon
Incheon 406-772, South Korea
Prof. S. Kim
School of Electrical Engineering
Korea University
Seoul 136-713, South Korea

DOI: 10.1002/adma.201201909

© 2012 WILEY-VCH Verlag GmbH & Co. KGaA, Weinheim

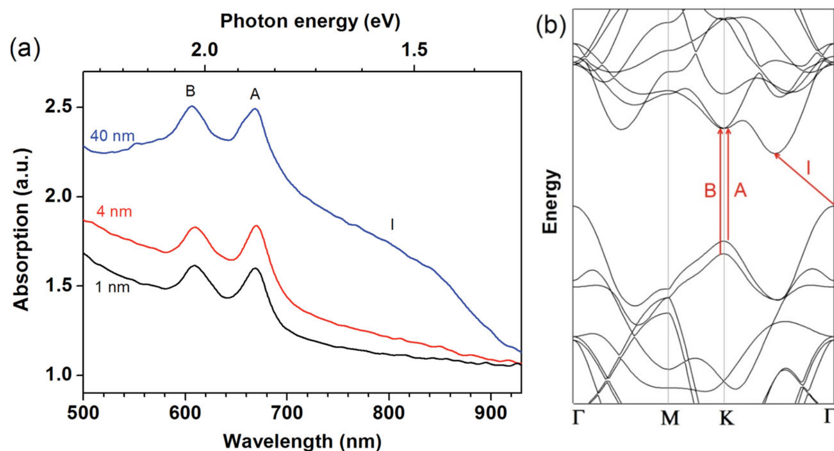

Figure 1. (a) Absorption spectra of MoS_2 crystals with three different thicknesses. Absorption peaks A and B correspond to the direct band transitions with the energy split from the valence band spin-orbital coupling. Broad absorption tail 'I' corresponds to the indirect band transition. As the MoS_2 crystal becomes thinner, this tail becomes weaker. (b) Band structure of bulk MoS_2. Direct band transitions A and B occur at K point. Indirect band transition I occurs between the valence band maximum at Γ point and the conduction band minimum.

absorption peaks – 'A' and 'B' – between 600 nm and 700 nm arising from the K point of the Brillouin zone.[13,14] Their energy differences are due to the spin-orbital splitting of the valence band, as indicated in Figure 1(b). For the thick MoS_2 flake (40 nm), an optical absorption tail – labeled 'I' – is observed through the indirect band transition at a wavelength longer than ~700 nm. However, as the thickness of MoS_2 flakes approached 1 nm, this absorption tail becomes weaker. This observation is consistent with the fact that single layer MoS_2 is a direct band gap semiconductor where the lowest energy interband transition occurs at the K point of the Brillouin zone.[13,14]

Next, multilayer MoS_2 TFTs are fabricated as shown in **Figure 2**(a) and their electrical transport properties are measured in a back-gated structure at room temperature. The thicknesses of MoS_2 flakes are in the range of 10–60 nm. Figures 2(c)-(d) show the transistor characteristics for multilayer MoS_2 TFTs (gate length ~3 μm, width ~7 μm, and thickness of MoS_2 channel ~20 nm) with a 50-nm-thick ALD Al_2O_3 gate insulator. The integration of high-κ dielectrics allows lower power consumption than SiO_2 ($\kappa = 3.9$) due to increased gate capacitance and dielectric screening of Coulomb scattering.[15] The measured current-voltage (I–V) behavior shows good agreement with a conventional long-channel NMOS transistor, exhibiting a linear triode regime at low drain voltages (V_{ds}) and a saturation regime at high V_{ds}. Unlike the reported 2D-crystal-based electronics, such as pristine graphene FETs[16,17] and single layer MoS_2 TFTs,[3] our transistors exhibit a current saturation at high V_{ds}. Saturation current at the "pinched-off" condition is independent of V_{ds} and is operated by the gate voltage according to the CMOS square-law model, in which the high output resistance in the saturation regime is a key factor to achieve a high voltage gain and to isolate output from the input signal in digital circuits. The representative multilayer MoS_2 TFT exhibits a maximum transconductance ($g_m = dI_d/dV_{gs}|_{V_{ds}=0.2V}$) of 3.12 μS, and an I_{on}/I_{off} of ~1×10^6. Note that the leakage current through the back gate in the operating regime is lower than the drain current by at least eight orders of magnitude. Based on the standard model of metal-oxide-semiconductor field-effect transistors (MOSFETs) and a parallel plate model of gate capacitance, the field effect mobility ($\mu_{eff} = Lg_m/(WC_{ox}V_{ds})$) extracted from our experimental transfer curves is >70 $cm^2V^{-1}s^{-1}$ in the linear regime (V_{ds} = 0.2 V). Interestingly, our multilayer MoS_2 transistors provide a higher μ_{eff} than those reported in conventional TFTs that are based on amorphous Si, low temperature poly-Si, or amorphous oxide semiconductors.[12]

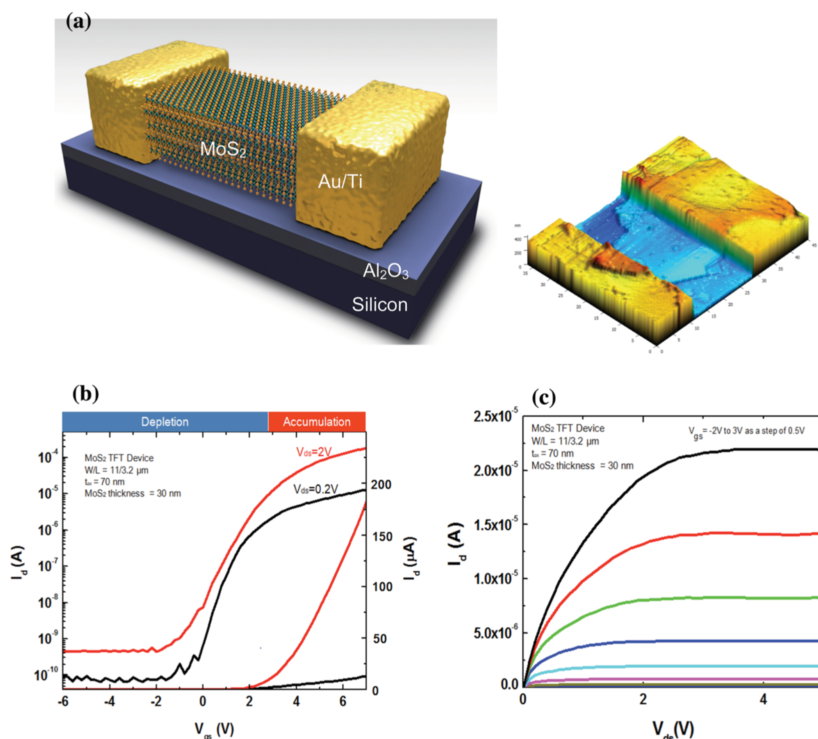

Figure 2. (a) Cross-sectional view and atomic force microscopy of multilayer MoS_2 TFTs consisting of an ALD Al_2O_3 gate insulator (50 nm), patterned Au electrodes (300 nm), and multilayer MoS_2 (thickness ~60 nm) as an active channel. (b) I–V characteristics of the multilayer MoS_2 (thickness ~35 nm) transistor with a gate length of 3.2 μm and MoS_2 width of 11 μm. The I_d-V_{gs} curves were measured under V_{ds} = 200 mV and 2 V. (c) I_d–V_{ds} curves recorded for various back-gated voltages with a step of 0.5 V.

Figure 3 shows the optoelectronic behavior of our multilayer MoS_2 phototransistors in the dark and under incident light

© 2012 WILEY-VCH Verlag GmbH & Co. KGaA, Weinheim
Adv. Mater. 2012,
DOI: 10.1002/adma.201201909

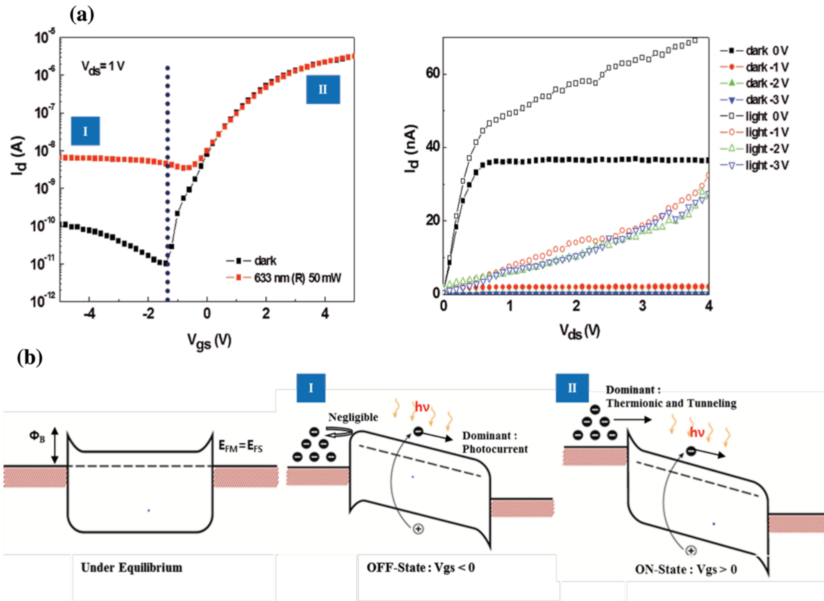

Figure 3. (a) Comparison of the *I*–*V* characteristics of an MoS_2 phototransistor under dark and light illumination conditions (λ_{ex} = 630 nm and power ~50 $mWcm^{-2}$). b) Energy-band diagram of a multilayer MoS_2 phototransistor with a Schottky barrier: Under equilibrium conditions, a Schottky barrier (Φ_B) between Ti/Au electrodes and an n-type semiconducting MoS_2 channel can be expressed as $\Phi_B = \Phi_M - \chi$, where χ is the electron affinity of MoS_2 and Φ_M is the Ti/Au metal workfunction. (i) Schematic OFF-state band diagram under light illumination, depicting the photogeneration of electron-hole pairs by the absorption of light inside MoS_2. (ii) Schematic ON-state band diagram in accumulation (V_{gs} > 0) with light. Photocurrent generated by light is negligible as thermionic and tunneling currents dominate channel current in the accumulation regime.

with a schematic energy band diagram illustrating the photogeneration process of the electron-hole pairs. When a tungsten lamp with λ = 630 nm and an intensity of 50 $mWcm^{-2}$ is illuminated on the MoS_2 channel at V_{ds} = 1 V, we observe a 10^3–fold increase in I_d in the "OFF-state"; yet, the accumulation current in the "ON-state" is independent of the incident light (see Figure 3(a)). Such opposing behavior can be explained by combining the dominant carrier transport mechanisms in the two distinct regimes: (i) photogenerated current, which dominates the depletion regime, and (ii) thermionic emission and tunneling current, which dominate the accumulation regime. Figure 3(b) shows an energy band diagram of a multilayer MoS_2 phototransistor with a Schottky barrier. Under equilibrium conditions, the Schottky barrier (Φ_B) between the Ti/Au electrodes and the n-type semiconducting MoS_2 channel can be expressed as $\Phi_B = \Phi_M - \chi$, where Φ_M is the Ti/Au metal workfunction and χ is the electron affinity of MoS_2. The schematic band diagram in the OFF-state under light illumination depicts the photogeneration of electron-hole pairs by the absorption of light inside the MoS_2. However, the schematic band diagram in the ON-state during accumulation (V_{gs} > 0) under light illumination shows the dominating effects of the thermionic and tunneling currents, and the negligible contribution of the photogenerated current.

Figure 4(a) schematically shows the carrier profile along the MoS_2 channel in the saturation regime of the transistor. The drain voltage primarily controls the carrier profile close to the drain region, which pinches off the channel at high source-drain voltages. This process leads to current saturation, as shown in Figure 2(c). When light is illuminated on the MoS_2 channel, carriers (both electrons and holes) are generated due to the band-to-band transition in addition to the electrons accumulated by the gate voltage. These photogenerated carriers modify the carrier profile along the channel particularly at the drain side where the carrier density is vanishingly small before illumination, as shown in Figure 4(b). The photogenerated electrons and holes move in opposite directions under the high source-drain electric field, leading to a generation current (I_G) in addition to the dark current. Hence, if P_{in} is the light power incident on the surface of the MoS_2 film, the residual power at a distance x from the surface is given by $P(x) = P_{in}e^{-\alpha x}$, where α is the absorption coefficient of the MoS_2 film at the incident photon energy. The amount of power absorbed by a slab of MoS_2 with thickness Δx at a distance x from the surface is $dR_a = -(dP/dx)\Delta x$. Then, the total power absorbed by the MoS_2 film of thickness d is $R_a = P_{in}(1-e^{-\alpha d})$. For $\alpha d << 1$, the absorbed power can be written as $R_a = P_{in}\alpha d$. Note that for a MoS_2 film with a thickness

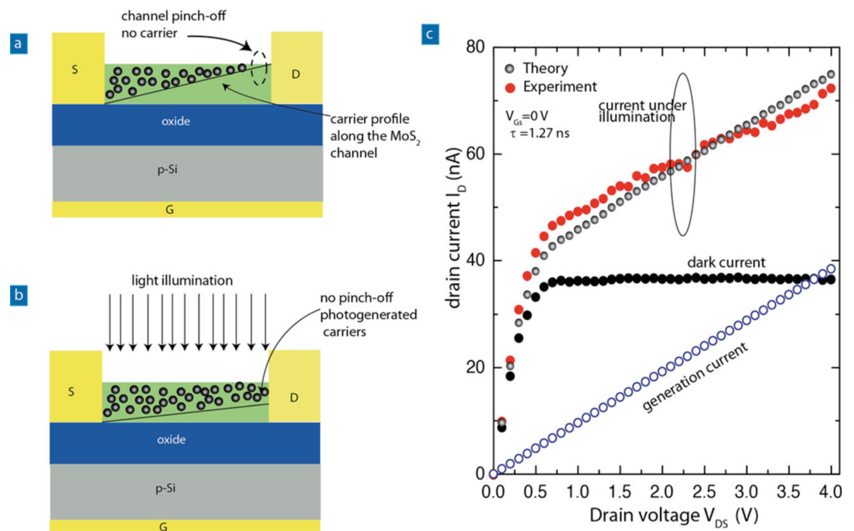

Figure 4. Schematic illustration of the carrier profile along the channel MoS_2 in the saturation regime (a) before and (b) after light illumination. Note that, due to photogenerated carriers after illumination, the channel does not pinch-off at the drain side. (c) Comparison between the theoretical model and the experimental measurements for the drain current under illumination.

© 2012 WILEY-VCH Verlag GmbH & Co. KGaA, Weinheim

of 30 nm and an absorption coefficient of $\alpha = 2 \times 10^5$ cm^{-1},[18] only 60% of the incident power is absorbed. If $h\nu$ is the energy of an incident photon, the number of electron-hole pairs generated per unit time per unit area is $G = R_a/h\nu$, where it is assumed that a single photon generates only one electron-hole pair. Defining τ as the carrier lifetime, the number of excess electron and hole generated per unit area is $\Delta n = \Delta p = G\tau$. Thus, the current due to these photogenerated carriers is $I_G = 2\Delta ne\mu(W/L)V_{ds}$, where e is the electronic charge, μ is the carrier mobility (assuming an identical value for electrons and holes), W is the device width, L is the device length, and V_{ds} is the applied source-drain voltage. The total drain current under illumination is therefore $I_D = I_D(\text{dark}) + I_G$. By comparing the experimentally measured current under illumination with the theory, we determine the carrier lifetime τ to be 1.27 ns, as shown in Figure 4(c). Note that the photogenerated current is not only proportional to V_{ds} (as in Figure 4 (c)), but it also varies linearly with the incident power, which agrees well with the experimental results (see inset of **Figure 5**(c)).

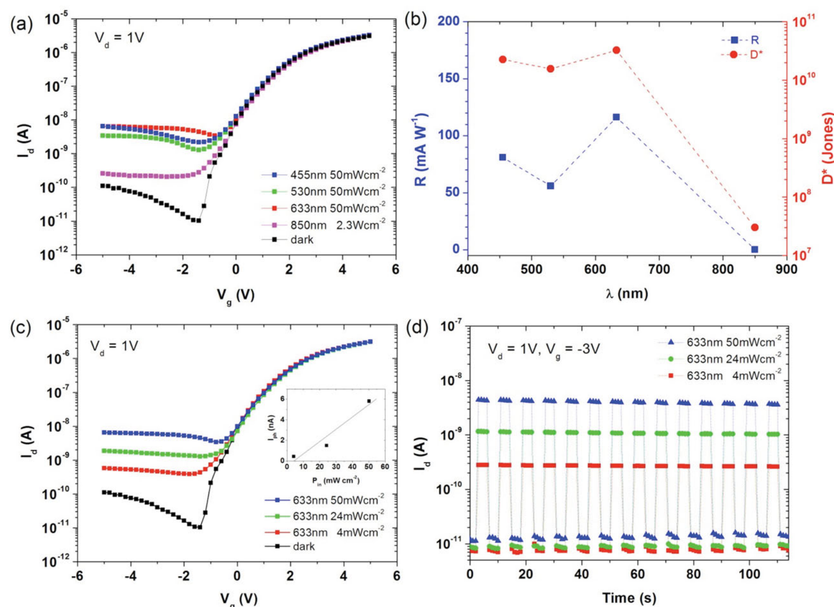

Figure 5. (a) Transfer characteristics of the phototransistor at different wavelengths. (b) Calculated responsivity and specific detectivity at different wavelengths. (c) Transfer characteristics of the phototransistor under visible light (633 nm) for different light intensities. Inset shows photocurrent response to light illumination (633 nm) for different light intensities. (d) Photocurrent as a function of light intensity at a wavelength of 633 nm.

As a next step, we also measure the dark currents and photocurrents of the MoS_2 phototransistor across a wide range of wavelengths and powers (Figure 5). In Figure 5(a), illuminating the phototransistor with monochromatic visible light (455 nm, 530 nm, and 633 nm) at a power density of 50 mWcm^{-2} increases the current up to almost three orders of magnitudes at an OFF-state gate bias. Under an infrared light (850 nm), a significantly higher power density (2.3 Wcm^{-2}) is needed to increase the current by an order of magnitude at the same gate bias. This low sensitivity for infrared light is related to the weak absorption tail of the indirect band gap semiconductor MoS_2 at the wavelength of 850 nm. The performance of the phototransistor as a photodetector can be evaluated by its figures of merit such as responsivity (R) and specific detectivity ($D*$).[19] Responsivity is a measure of the electrical response to light and is given by $R = I_{ph}/P_{in}$, where I_{ph} is the photocurrent flowing in a detector and P_{in} is the incident optical power. Specific detectivity is a measure of detector sensitivity and, assuming that shot noise from dark current is the major contributor to the total noise, it is given by $D* = RA^{1/2}/(2eI_d)^{1/2}$, where R is the responsivity, A is the area of the detector, e is the unit charge, and I_d is dark current.[20] Figure 5(b) shows the calculated R and $D*$ of the phototransistor at different wavelengths. For visible light, R and $D*$ exist in the range of 50–120 mAW^{-1} and 10^{10}-10^{11} Jones, respectively. However, the R and $D*$ of infrared are significantly reduced to 9×10^{-2} mAW^{-1} and 5×10^7 Jones, respectively. Although our MoS_2 phototransistors show much inferior performances to silicon photodiodes (R ~ 300 AW^{-1} and $D*$ ~10^{13} Jones),[6,21] their performance is better than phototransistors based on graphene (R ~1 mAW^{-1} at V_g = 60 V)[22] or single layer MoS_2 ($R \leq 7.5$ mAW^{-1} at V_g = 50 V).[3] Future work involving optimizing the device architecture and processing will greatly enhance the performance of our MoS_2 phototransistors.

To further characterize our phototransistors, the illumination intensity-dependence of the transfer curves is measured under a visible light (633 nm). As shown in Figure 5(c), as the illumination intensity increases from 4 mWcm^{-2} to 50 mWcm^{-2}, the photocurrent also increases. Since the linear device response to the incident light intensity is important, a plot of photocurrent as a function of illumination intensity is shown in the inset of Figure 5(c) at V_{ds} = 1 V and V_{gs} = –3 V. The good linear output between the photocurrents and the illumination intensity indicates that photocurrent is determined by the number of photo generated carriers under illumination. From the slope of the linear fit, a responsivity of ~12 mAW^{-1} is obtained, which is consistent with the result in Figure 5(b). In addition, the time-resolved photoresponse is measured for multiple illumination cycles, as depicted in Figure 5(d). Although an accurate response time is not measurable within our experimental setup, a nearly identical response was observed for multiple cycles, which demonstrates the robustness and reproducibility of our phototransistors.

In conclusion, we fabricated phototransistors based on multilayer MoS_2 flakes and investigated their optoelectronic properties, including their photogeneration and photoresponse in wide-spectrum ranges. Due to its relatively small bandgap (~1.3 eV), multilayer MoS_2 can potentially be integrated into various optical sensors that require a broad range of spectral responses from UV to near-IR, as an alternative to the conventional GaN-, Si-, and GaAs-based photodetectors. Furthermore, the high photoresponsivity (>100 mAW^{-1}) of multilayer MoS_2 phototransistors, combined with their optical stability (i.e., no-shift in the threshold voltage) under illumination, can be attractive for a variety of industrial applications, including touch sensor panels, image sensors, solar cells, and communication devices.

© 2012 WILEY-VCH Verlag GmbH & Co. KGaA, Weinheim
Adv. Mater. 2012, DOI: 10.1002/adma.201201909

Experimental Section

To obtain the optical absorption in MoS_2 flakes, absorption differences between a glass substrate and the MoS_2 flakes were measured using an absorption spectroscopy in a microscope setup. For the fabrication of MoS_2 transistors, an amorphous Al_2O_3 dielectric layer of ~50 nm in thickness was deposited on a highly-doped p-type Si wafer (resistivity $<5 \times 10^{-3}$ Ω·cm) by atomic layer deposition process using trimethylaluminum (TMA, UP Chemical Co. Ltd., South Korea) and H_2O as a precursor and a reactant, respectively. The deposition temperature was maintained at 300 °C and the gas injection schedule for one cycle of deposition were 0.5/10/1.5/15 seconds for the TMA/N_2/H_2O/N_2 gases. Multilayer MoS_2 flakes were mechanically exfoliated from bulk MoS_2 crystals and transferred on the substrate. Electrical contacts (100 μm × 100 μm) were patterned on top of MoS_2 flakes using conventional lift-off technique. Ti (10 nm) and Au (300 nm) were deposited by electron-beam evaporation at room temperature. The device was then annealed at 200 °C in a vacuum tube furnace for 2 hours (100 sccm Ar and 10 sccm H_2) to remove resist residue and to decrease contact resistance. The thickness of MoS_2 was measured using an AFM (Nanoscope III, Digital Instruments-Veeco, USA). Electrical characterizations were carried out with current-voltage measurements (Keithley, Semiconductor Characterization System 4200-SCS).

Supporting Information

Supporting Information is available from the Wiley Online Library or from the author.

Acknowledgements

W. Choi and M. Y. Cho contributed equally to this work. W. Choi acknowledges the partial financial support of the Research Program 2012 of Kookmin University in South Korea.

Received: May 11, 2012
Revised: July 11, 2012
Published online:

[1] B. Radisavljevic, A. Radenovic, J. Brivio, V. Giacometti, A. Kis, *Nat. Nanotechnol.* **2011**, *6*, 147.
[2] Y. Yoon, K. Ganapathi, S. Salahuddin, *Nano Lett.* **2011**, *11*, 3768.
[3] Z. Yin, H. Li, H. Li, L. Jiang, Y. Shi, Y. Sun, G. Lu, Q. Zhang, X. Chen, H. Zhang, *ACS Nano* **2012**, *6*, 74.
[4] S. Kim, A. Konar, W.S. Hwang, J. H. Lee, J. Lee, J. Yang, C. Jung, H. Kim, J. B. Yoo, J. Y. Choi, Y. W. Jin, S. Y. Lee, D. Jena, W. Choi, K. Kim, *Nat. Commun.* **2012**, in press.
[5] K. Natori, *J. Appl. Phys.* **1994**, *76*, 4879.
[6] X. Gong, M. Tong, Y. Xia, W. Cai, J. S. Moon, Y. Cao, G. Yu, C.-L. Shieh, B. Nilsson, A. J. Heeger, *Science* **2009**, *325*, 1665.
[7] D. J. Late, B. Liu, H. S. S. R. Matte, C. N. R. Rao, V. P. Dravid, *Adv. Funct. Mater.* **2012**, *22*, 1894.
[8] D. J. Late, B. Liu, H. S. S. R. Matte, V. P. Dravid, C. N. R. Rao, *ACS Nano* **2012**, *6*, 5635.
[9] A. Ayari, E. Cobas, Q. Ogundadegbe, M. S. Fuhrer, *J. Appl. Phys.* **2007**, *101*, 014507.
[10] V. Podzorov, M. E. Gershenson, Ch. Kloc, R. Zeis, E. Bucher, *Appl. Phys. Lett.* **2004**, *84*, 3301.
[11] S. Y. Han, D. C. Kim, B. Cho, K. S. Jeon, S. M. Seo, M. S. Seo, S.-W. Jung, K. Jeong, W. K. Kim, S.-H. Yang, N.-H. Kim, J. Song, H.-S. Kong, H. G. Kim, *J. Soc. Inf. Display* **2011**, *19*, 855.
[12] S. Jeon, S.-E. Ahn, I. Song, C.-J. Kim, U.-I. Chung, E. Lee, I. Yoo, A. Nathan, S. Lee, J. Robertson, K. Kim, *Nat. Mater.* **2012**, *11*, 301.
[13] A. Splendiani, L. Sun, Y. Zhang, T. Li, J. Kim, C. Chim, G. Galli, F. Wang, *Nano Lett.* **2010**, *10*, 1271.
[14] K. F. Mak, C. Lee, J. Hone, J. Shan, T. F. Heinz, *Phys. Rev. Lett.* **2010**, *105*, 136805.
[15] D. Jena, A. Konar, *Phys. Rev. Lett.* **2007**, *98*, 136805.
[16] J. Kedzierski, *IEEE Trans. Electron. Dev.* **2008**, *55*, 2078.
[17] X. Li, X. Wang, L. Zhang, S. Lee, H. Dai, *Science* **2008**, *319*, 1229.
[18] R. F. Frindt, A. D. Yoffe, *Proc. Roy. Soc. A* **1963**, *273*, 69.
[19] G. Konstantatos, E. H. Sargent, *Nat. Nanotechnol.* **2010**, *5*, 391.
[20] A. R. Jha, *Infrared Technology*, Wiley, New York **2000**.
[21] Y. Guo, G. Yu, Y. Liu, *Adv. Mater.* **2010**, *22*, 4427.
[22] F. Xia, T. Mueller, Y. Lin, A. Valdes-Garcia, P. Avouris, *Nat. Nanotechnol.* **2009**, *4*, 839.

© 2012 WILEY-VCH Verlag GmbH & Co. KGaA, Weinheim